Ytterbium-based bioprobes for near-infrared two-photon scanning laser microscopy imaging.

Anthony D'Aléo, Adrien Bourdolle, Sophie Brustlein, Teddy Fauquier, Alexei Grichine, Alain Duperray, P. L. Baldeck, Chantal Andraud, Sophie Brasselet, Olivier Maury

NIR-to-NIR bioimaging DOI: 10.1002/anie.200((will be filled in by the editorial staff))

Ytterbium based Bioprobes for *NIR*-to-*NIR* Two Photon Scanning Laser Microscopy Imaging.[**]

Anthony D'Aléo, Adrien Bourdolle, Sophie Brustlein, Teddy Fauquier, Alexei Grichine, Alain Duperray, Patrice L. Baldeck, Chantal Andraud [*], Sophie Brasselet [*],and Olivier Maury [*]

This paper is dedicated to Dr. Hubert Le Bozec at the occasion of his 60th birthday.

For decades, optical microscopy has been an essential tool for biological imaging, and more recently luminescence-based techniques have gained widespread utilization for medical analyses and diagnostics.[1] Conventional one-photon microscopy using commercial bio-probes or fluorescent proteins generally proceeds using excitation wavelength in the UV or visible and detection in the visible spectral range. These microscopy configurations will be referred to as *UV*-to-*visible* or *visible*-to-*visible* according to the *excitation-to-detection* spectral ranges. Since biological tissues strongly absorb and scatter UV-visible light, such configurations are restricted to surface bio-imaging experiments *e.g.* 2D cell imaging. On the other hand, the transparency of biological tissues in the near infra-red (NIR) between 700 and 1200 nm, a region called biological window, allows in-depth imaging in this spectral range.[2] Therefore, numerous academic and industrial research endeavors are currently focused on the improvement of microscopy techniques and on the design of new luminescent bio-probes featuring *both* excitation and emission in this NIR spectral range. Microscopy in this *NIR-to-NIR* configuration will enable in depth imaging in thick tissues and several bio-probes (cyanine, (aza)-bodipy) combining NIR excitation and emission have been developed and commercialized this last decade.[3] However in these cases, the small Stokes shift between the excitation and the optimal collection range of emitted light is a real technical drawback for microscopy because of the need to cleanly separate the emission from the excitation. Nonlinear biphotonic excitation, that is the simultaneous absorption of two photons of half energy typically in the NIR region, inherently introduces a larger Stokes shift and is therefore an elegant way to circumvent this drawback.[4] However, up to now, all the designed chromophores exhibit an emission in the visible spectral range, and the currently available biphotonic microscopes work in this *two photon NIR*-to-*visible* configuration with detection wavelength shorter than the incident laser one.[4,5]

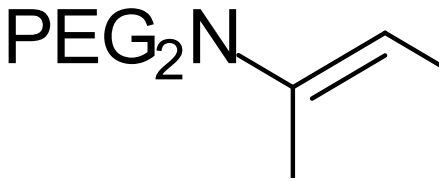

Figure 1. Structure of the target complexes.

In this context, lanthanide complexes and particularly NIR emitters like ytterbium, and neodymium are known to exhibit very large pseudo-Stokes shift,[6a,b] and are therefore potentially well suited for such two photon *NIR*-to-*NIR* imaging purpose. In spite of their generally low luminescence quantum yield, such complexes have already been used for NIR bio-imaging applications but with a classical one photon excitation generally localized in the UV-visible up to 550-600 nm.[6,7] The sensitization of lanthanide luminescence by two-photon absorption is currently a challenging field of research but so far, most endeavors were focused on terbium and europium emitting in the green and red, respectively.[6a,8] With regard to NIR emitters, the proof of concept of ytterbium two-photon sensitization

[*] Dr. A. D'Aléo, Dr. A. Bourdolle, Dr. P.L. Baldeck, Dr. C. Andraud, Dr. O. Maury University Lyon 1, ENS Lyon, CNRS UMR 5182, 46 allée d'Italie 69364 Lyon, France. olivier.maury@ens-lyon.fr; chantal.andraud@ens-lyon.fr.

Dr. S. Brustlein, Dr. S. Brasselet Institut Fresnel, CNRS UMR 6133, Université Aix Marseille III, Ecole Centrale de Marseille, Domaine Universitaire St Jérôme, 13397 Marseille cedex 20, France. sophie.brasselet@fresnel.fr
Dr. A. Grichine, Dr. A. Duperray ,Institut Albert Bonniot, INSERM-U823-CHU Grenoble-EFS, Université Joseph Fourier - Grenoble I, BP170, 38042 Grenoble, France.
Dr. T. Faulquier Institut de Génomique Fonctionnelle de Lyon, Université de Lyon, CNRS, INRA, Ecole Normale Supérieure de Lyon, 46 allée d'Italie, 69364 Lyon, France.

[**] Authors are grateful to Drs Y. Guyot and A. Brenier (LPCML, university of Lyon) for their help in the NIR luminescence decays measurements. We also thank F. Albrieux, C. Duchamp and N. Henriques (University of Lyon) for the assistance and access to the High Resolution Mass Spectrometry facility.

Supporting information for this article is available on the WWW under http://www.angewandte.org or from the author.

has been first described in the early 2000s by Lakowicz *et al.*.[9] Recently, Wong and co-workers have reported an ytterbium complex that exhibit exceptional luminescence properties in water with remarkable two-photon cross-section.[10] Interestingly, this complex was successfully used as bio-probe to image HeLa cells by two-photon microscopy technique, but working in the classical *NIR*-to-*visible* configuration with detection in the residual ligand centered emission.

In this article, we report on the proof-of-concept of *two-photon NIR-to-NIR* microscopy. To that end, we designed water soluble ytterbium complexes, containing extended π-conjugated skeleton suitable for two-photon excitation and meanwhile, we built up an unconventional two-photon *NIR*-to-*NIR* microscopy set-up.

The target complexes (Figure 1) need to fulfill some requirements to be used as bio-probe, ideally efficient two-photon antenna, high thermodynamical and kinetic stability and good photophysical properties. For initial spectroscopy and microscopy experiments, we chose to use the previously described[11] **Yb^1** complex containing bis-PEGamino-(phenylethynyl)-dipicolinic ligands in spite of its limited water stability.[12] In a second time, the analogous macrocylic complex, **Yb^2** based on the triaza-cyclononane plateform[13,14] was designed to increase the stability in biological medium (SI for synthetic details and characterizations).

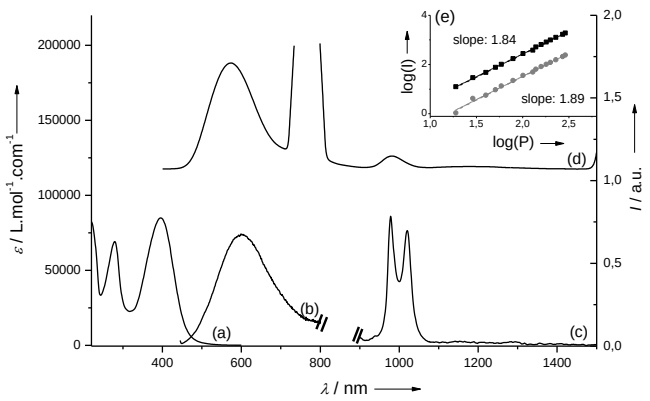

Figure 2. Photophysical data of **Yb^1** in water solution: (a) absorption spectrum (scale on the left), (b) residual CT fluorescence and (c): NIR emission (λ^{ex}= 380 nm) (scale on the right), (d): Uncorrected two photon induced luminescence spectrum (λ^{ex} = 760 nm) (scale on the right). Inset (e) variation of the two-photon luminescence intensity with the incident laser power at 573 nm (■) and 981 nm (●).

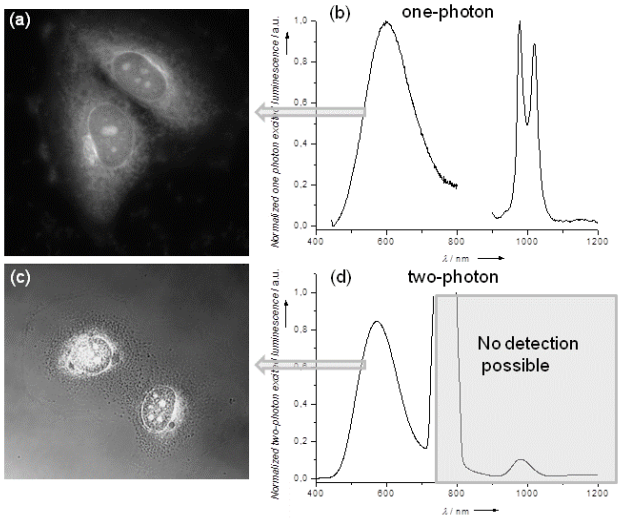

Figure 3. Imaging of the fixed cells stained with **Yb^1** using a conventional microscope: (a) one photon imaging using inverted wide field microscope (λ^{ex} = 450-490 nm, visible detection) (b) one- and two-photon emission spectra; (c) two-photon NIR-to-visible imaging laser scanning microscope,(λ^{ex} = 760 nm, 491-673 nm detection).

In both cases, the UV-visible absorption spectra exhibit a broad intense transition at 400 nm, assigned to an intraligand charge transfer transition (ILCT) from the dialkylamino donnor part to the chelated dipicolinic electron-withdrawing fragment (Figures 2 and S2). As already observed,[11] the steady-state luminescence spectra obtained by excitation in this ILCT transition is composed of two emission bands: (i) the characteristic ytterbium (III) emission, arising from the $^2F_{5/2} \rightarrow {}^2F_{7/2}$ (980 nm) transition in the NIR spectral range and (ii) the broad residual ILCT emission around 600 nm, indicating that the energy transfer to the central metal ion is not complete. The luminescence lifetime associated to the NIR transition was found to be perfectly mono-exponential, with a value of 0.34 and 3 μs for **Yb^1** and **Yb^2** respectively (Figure S3), this later value being in the range of best complexes already reported in water.[10,15] The strong improvement between the two complexes **Yb^1** and **Yb^2** featuring similar antenna can be ascribed to the increased stability of the macrocyclic derivative.[13] Under fs-Ti:Sa laser irradiation in the 700-900 nm spectral range (Figure S4), an identical luminescence profile is obtained (Figure 2d) with NIR emission observed at a longer wavelength compared to that of the incident laser one (*i.e.* unusual spectral configuration for TPA induced luminescence with $\lambda^{det} > \lambda^{ex}$). The quadratic dependence of both residual ILCT and Yb(III) emission intensity versus the laser power (Figure 2e) unambiguously established that the NIR Yb(III) emission is that sensitized by a two-photon antenna effect. The two-photon cross-sections could not be accurately determined due to the weak luminescence quantum yields of both residual ILCT and Yb(III) emissions (< 1%), and to the lack of calibration of the TPA experimental set-up in the NIR spectral range. However in a first approximation, these cross-sections should lie in the same range than that of the europium or lutetium analogous estimated to 775 and 500 GM at 740 nm, respectively.[11] Therefore the TPA-induced NIR emission of ytterbium is particularly interesting for in-depth bio-imaging experiments since both excitation (750-850 nm) and emission (980 nm) are localized in the biological transparency window (*NIR*-to-*NIR* configuration).

Conventional one- and two-photon microscopy imaging experiments were carried out using commercially available epifluorescence and confocal microscopes with either a one-photon excitation in the visible or a two-photon excitation at 760 nm (fs-Ti:Sapphire laser). The complex **Yb^1** was incubated with fixed T24 human cancer cells. The one-photon microscopy image (Figure 3a) reveals that the complex successfully stained the cell and localized preferentially in the perinulear areas or nucleoli as already observed for related europium complexes.[12] The conventional two-photon imaging experiments (Figure 3c) were carried out in the *NIR*-to-*visible* configuration using a visible detection at lower wavelength than the TPA excitation ($\lambda^{det} < \lambda^{ex}$). As expected, this image is very similar to the one-photon one, but the signal-to-noise ratio is lower because the background fluorescence is dramatically reduced using a two-photon excitation. Unfortunately, it was not possible to record

any image at the 950-1050 nm emission band since conventional biphotonic microscopes contain optical filtering schemes which do not allow the *NIR*-to-*NIR* configuration (that is detection of $\lambda^{det} > \lambda^{ex}$ with both λ^{ex} and λ^{det} in the NIR range). Additionally, the sensitivity of the standard PMT detectors of the confocal microscope is very low at 980 nm. To tackle these limitations, we developed our own biphotonic microscopy set-up based on adequate optical filtering.

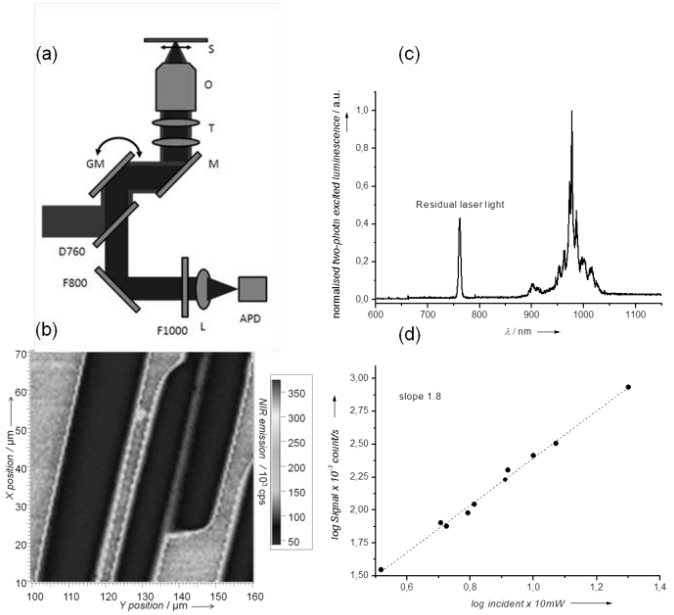

Figure 4. (a) Experimental setup for two photon NIR-to-NIR imaging. O: objective; T: telescope; M: protected silver mirror; GM: galvanometric mirrors; D760: dichroic mirror (FF720-SDi01, Semrock); F800 and F1000: interference filters (800DF50 and 1000DF50, Omega Optical); L: lens; APD: Avalanche Photodiode. (b), imaged two-photon imaging. (b) Two-photon scanning image of a thin film of **Yb[1]** on a glass substrate, using a 1000 nm detection wavelength. (c) Spectrum measured in a bright region of the image of (b) (a high pass filter at 850 nm is used before the spectrometer). (d) Incident power dependence of the fluorescence signal recorded in the 1000 nm spectral detection range.

The two-photon *NIR*-to-*NIR* imaging microscopy set-up (Figure 4a) consists in focusing an incident pulsed Ti-sapphire laser light (100 fs, 80 MHz, 760 nm wavelength) through a high numerical aperture objective (NA 1.15, water immersion). Images are formed using a galvalnometric scanning over typical regions of 100 µm x100 µm in the sample plane. To reject as much as possible the incident laser light in the detection channel around 1000 nm, the laser is reflected on a dichroic mirror which transmits the fluorescence emission in the epi descanned detection path. The emission is further filtered by two interference filters, and focused on an avalanche photodiode working in the photon counting mode. Validation experiments were first carried out using a thin film of **Yb[1]** spread on a glass plate as substrate (Figure 4b). Regions where the film is present are clearly visible with a high signal to background ratio comparing to the glass substrate. Both the spectrum of emission (Figure 4c) and the incident intensity dependence (Figure 4d) ascertain the detection of NIR light around 1000 nm in the two-photon mode.

As preliminary to the imaging experiments, the influence of this *NIR*-to-*NIR* configuration on the depth of penetration in a scattering sample was studied. To that end, the complex **Yb[1]** was dissolved in Intralipids solutions of different concentrations, mimicking the scattering ability of the biological media and irradiated by a biphotonic excitation. The variation of the normalized emission intensity in the visible (600 nm) and in the NIR (1000 nm) was measured simultaneously as a function of the depth of the incident laser focusing position (Figure 5a). As anticipated, the visible emission is more affected by scattering than the NIR one: at a depth of 100 µm in a strongly scattering medium, almost no visible light is detected whereas more than 20 % of the NIR light remains available for imaging purpose. These data are in agreement with recent results comparing the influence of the detection wavelength for a given TPA excitation[16] both obtained in a classical TPA configuration ($\lambda^{ex} > \lambda^{det}$). Note that the data shown in Figure 5 are normalized, and usually the NIR detection range exhibits fewer signal than in the visible range, due to the lower efficiency of both the imaging set-up and the luminescence quantum yield of the complex in this spectral range. Nevertheless, all these experiments unambiguously emphasize the interest of the *NIR*-to-*NIR* configuration for in-depth imaging purposes.

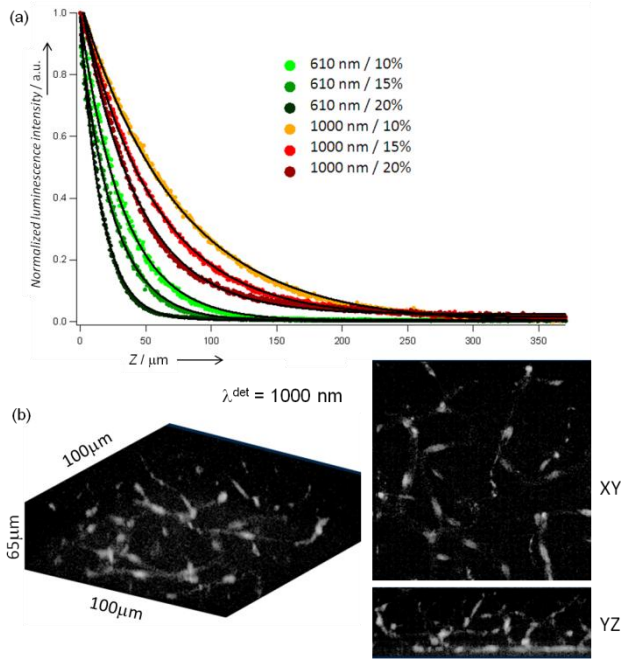

Figure 5. a) Variation of the normalized luminescence intensity of **Yb[1]** at 610 nm (green) or 1000 nm (red) with the depth of the 760 nm TPA excitation in two Intralipids solutions of different concentrations (10%, 15%, 20%) mimicking different scattering strengths. b) Biphotonic scanning microscopy 3D imaging using the home made set-up (λ^{ex} = 760 nm) of mouse brain slice stained with **Yb[2]** with detection at 1000 nm (incident power 25mW). Sections of the 3D images of the aforementioned image.

In order to check the potentialities of this two photon *NIR*-to-*NIR* configuration, thick tissues imaging experiments were undertaken. Mouse brain capillary vessels were imaged in-depth using the **Yb[2]** as luminescent probes.[17] A phosphate buffer solution of the complex ([C] ~ 10^{-4} mol.L^{-1}) was directly perfused in the heart of a mouse. Brains were quickly dissected, post-fixed, and slices (100 µm thickness) were cut and conserved between two glass plates. These mouse brain slices were successfully imaged using a biphotonic excitation (λ^{ex} = 760 nm) and the 3D blood capillary network is observed using the NIR-to-NIR configuration with a detection at 1000 nm (Figure 5b). This image was recorded at higher laser power to compensate for the lower imaging efficiency in this

spectral range. Even though the recorded signal is weak for the reasons given above, it shows stained blood vessels with reasonable signal to noise ratio up to 80 μm depths in strongly scattering samples. The integration time of 50 μs per pixel, which is essentially chosen to ensure a high signal to noise ratio, could be even more increased to reach larger imaging depth. This would lead to longer time scales imaging, however it is possible to reach faster dynamics by using a higher incident power. This result therefore unambiguously establishes the proof-of-concept of two-photon *NIR*-to-*NIR* imaging.

In conclusion, this article demonstrates the feasibility of in-depth imaging of strongly scattering thick tissue *e.g.*, the vascular network of mouse brain, by two-photon scanning microscopy in an unprecedented *NIR*-to-*NIR* configuration. To that end, we developed a new biphotonic set-up and we designed a macrocyclic ytterbium complex functionalized by two-photon antenna combining appropriate stability and efficiency in water. Further studies are currently conducted to improve the two-photon brightness of such probes and to expand the scope of this *NIR*-to-*NIR* biphotonic microscope.

Experimental Section

Synthetic procedures and characterizations, spectroscopic and microscopic experimental details and biological samples preparation are described in supporting information.

Received: ((will be filled in by the editorial staff))
Published online on ((will be filled in by the editorial staff))

Keywords: Biphotonic microscopy · NIR-to-NIR configuration· Lanthanide complex · Ytterbium complex · Bioimaging

[1] V. Ntziachriostos, *Nature Meth.* **2010**, 7, 603-614.
[2] J. V. Frangioni, *Curr. Op. Chem. Biol.* **2003**, *7*, 626-634
[3] a) K. Kiyose, H. Kojima, T. Nagano, *Chem. Asian J.* **2008**, *3*, 506-515; b) S. Achilefu, *Angew. Chem. Int. Ed.* **2010**, *49*, 9816-9818; c) H.S. Choi, K. Nasr, S. Alyabyev, D. Feith, J. H. Lee, S. H. Kim, Y. Ashitate, H. Hyun, G. Patonay, L. Strekowski, M. Henary, J. V. Frangioni, *Angew. Chem. Int. Ed.* **2011**, *50*, 6258-6263
[4] a) W. R. Zipfel, R. M. Williams, W. W. Webb, *Nat. Biotechnol.* **2003**, *21*, 1369-1377; b) K. Konig, *J. Microsc.* **2000**, *200*, 83-104.
[5] a) H. M. Kim, B. R. Cho, *Acc. Chem. Res.* **2009**, *42*, 863-872; b) G. S. He, L.-S. Tan, Q. Zheng, P.N. Prasad, *Chem. Rev.* **2008**, *108*, 1245-1330.
[6] a) S. V. Eliseeva, J.-C. G. Bünzli, *Chem. Soc. Rev*., **2010**, *39*, 189–227 ; b) J.-C. G. Bünzli, S. V. Eliseeva *J. Rare Earth*, **2010**, *28*, 824–842; c) S. Pandya, J. Yu, D. Parker *Dalton Trans.* **2006**, 2757; d) S. Faulkner, S. J. A. Pope, B. P. Burton-Pye, *Appl. Spectrosc. Rev.* **2004**, *40*, 1.
[7] For recent examples see: a) H. He, L. Si, Y. Zhong, M. Dubey *Chem. Commun.* **2012**, *48*, 1886-1888 and references therein.
[8] For reviews see: a) C. Andraud, O. Maury, *Eur. J. Inorg. Chem.* **2009**, 4357-4371; b) Y. Ma, Y. Wang, *Coord. Chem. Rev.* **2010**, *254*, 972–990.
[9] G. Piszczek, I. Gryczynski, B. P. Maliwal, J. R. Lakowicz *J. Fluoresc.* **2002**, *12*, 15-17.
[10] T. Zhang, X. Zhu, C. C. W. Cheng, Kwok, W.M.; Tam, H. L.; Hao, J.; Kwong, D.W.J.; Wong, W.K.; Wong, K.L., *J. Am. Chem. Soc.* **2011**, *133*, 20120-20122.
[11] a) A. D'Aléo, A. Picot, A. Beeby, J. A. G. Williams, B. Le Guennic, C. Andraud, O. Maury, *Inorg. Chem.* **2008**, *47*, 10258-10268; b) A. D'Aléo, A. Picot, P. L. Baldeck, C. Andraud, O. Maury, *Inorg. Chem.* **2008**, *47*, 10269-10279.
[12] A. Picot, A. D'Aléo, P. L. Baldeck, A. Grichine, A. Duperray, C. Andraud, O. Maury *J. Am. Chem. Soc.* **2008**, *130*, 1532-1533.
[13] G. Nocton, A. Nonat, C. Gateau, M. Mazzanti, *Helv. Chem. Acta*, **2009**, *92*, 2257-2273.
[14] A. Bourdolle, M. Allali, J.-C. Mulatier, B. Le Guennic, J. Zwier, P. L. Baldeck, J.-C.G. Bünzli, C. Andraud, L. Lamarque, O. Maury *Inorg. Chem.* **2011**, *50*, 4987-4999.
[15] For mono-metallic complexes see : a) E. G. Moore, J. Xu, S. C. Dodoni, C. J. Jocher, A. D'Aléo, M. Seitz , K. Raymond, *Inorg. Chem.* **2010**, *49*, 4156-4166 ; b) A. Nonat, D. Imbert, J. Pecaut, M. Giraud, M. Mazzanti, *Inorg. Chem.* **2009**, *48*, 4207-4218 ; c) S. Comby, D. Imbert, C. Vandevyver, J.-C. G. Bünzli, *Chem. Eur. J.* **2007**, *13*, 936-944 ; d) M. H.V. Werts, R. H. Woudenberg, P. G. Emmerink, R. van Gassel, J.W. Hofstraat, J. W. Verhoeven, *Angew. Chem. Int. Ed.* **2000**, *39*, 4542-4544
[16] a) P. M. Allen, W. Liu, V. P. Chauhan, J. Lee, A. Y. Ting, D. Fukumura, R. K. Jain, M. G. Bawendi, *J. Am. Chem. Soc.* **2010**, *132*, 470-471; b) D. Kobat, M. E. Durst, N. Nishimura, A. W. Wong, C. B. Schaffer, C. Xu, *Opt. Exp.* **2009**, 13354-1364.
[17] No images could be obtained using **Yb[1]** as probe certainly due to its too low stability in the small animal.

Entry for the Table of Contents

NIR-to-NIR bioimaging

A. D'Aléo, A. Bourdolle, S. Brustlein, T. Fauquier, A. Grichine, A. Duperray, P. L. Baldeck, C. Andraud*, S. Brasselet*, O. Maury*_____ **Page – Page**

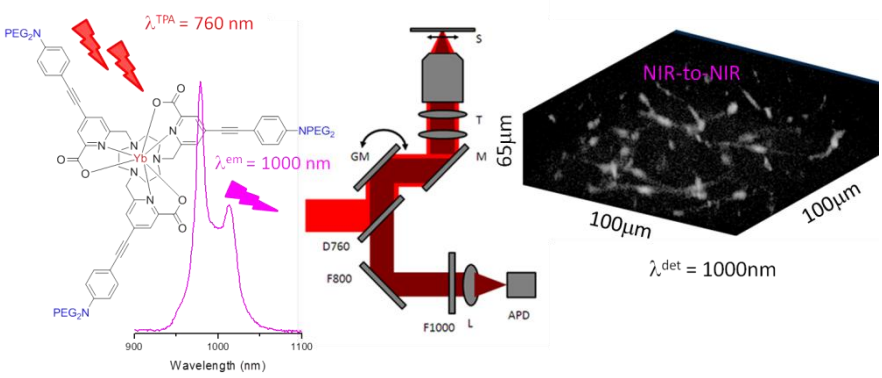

Ytterbium based Bioprobes for NIR-to-NIR Two Photon Scanning Laser Microscopy Imaging.

The design and photophysical characterization of a new highly stable macrocyclic ytterbium complex featuring two-photon antenna ligand is described. The biphotonic sensitization of the NIR Yb(III) luminescence and the conception of an unconventional *NIR-to-NIR biphotonic microscope* allow performing in-depth imaging of thick tissues.

Supporting information for:

Ytterbium based Bioprobes for NIR-to-NIR Two Photon Scanning Laser Microscopy Imaging.

Anthony D'Aléo, Adrien Bourdolle, Sophie Brustlein, Teddy Fauquier, Alexei Grichine, Alain Duperray, Patrice L. Baldeck, Chantal Andraud, Sophie Brasselet, and Olivier Maury

Synthesis

Scheme S1: Synthesis of the ligand $\mathbf{L^2}$ and related $\mathbf{Yb^2}$ complex

General. 4-ethynyl-N,N bis(2-(2-(2-methoxyethoxy)ethoxy)ethyl)aniline (**1**), [1] and methyl 6-(hydroxymethyl)-4-iodopicolinate (**2**) [2] were prepared following the published procedures, all other starting materials were commercially available. All solvents for synthesis were analytic grade. NMR spectra (^{1}H, ^{13}C) were recorded at room temperature on a BRUKER Advance operating at 500.10 MHz and 125.75 MHz for ^{1}H and ^{13}C, respectively. Data are listed in parts per million (ppm) and are reported relative to tetramethylsilane (^{1}H, ^{13}C); residual solvent peaks of the deuterated solvents were used as internal standard. UV/Vis absorption measurements were recorded on an absorption spectrometer JASCO V670. Low resolution mass spectrometry was carried out on an Agilent 1100 Series LC/MSD apparatus. The ligand under its trimester form (**5**) was analyzed by RP-HPLC using a Waters Alliance 2695 system coupled with Waters 996 photodiode array detector and Micromass ZQ Waters 2000 mass spectrometer. Procedure developed was 0.1% formic acid in water / acetonitrile as mobile phase using XBridgeTM C18, 3.5 µm, 4.6 × 100 mm as column. High resolution Mass spectrometry (HRMS) was performed using a Bruker MicroTOF-Q II, apparatus (precision 1-5 ppm) equipped with an electrospray source using highly diluted samples (1-2 mg/ mL) in a methanol/dichloromethane/water/formic acid mixture (46.1/38.4-15.4-0.1 v/v).

3. In a 100 mL schlenk flask under argon, **1** (1.100 g, 2.68 mmol, 1.3 eq) and **2** (590 mg, 2.01 mmol, 1 eq) were dissolved in a mixture of THF (20 mL) and triethylamine (20 mL). After degassing by argon bubbling, $PdCl_2(PPh_3)_2$ (141 mg, 0.201 mmol, 0.1 eq) and copper iodide (76 mg, 0.402 mmol, 0.2 eq) were added. The solution was stirred at RT for 20 h. The solution volume was extended to 100 mL by addition of THF, filtered, and solvents were evaporated. The residue was dissolved in DCM (50 mL) washed with saturated NH_4Cl (2 × 100 mL), water (100 mL), and dried (Na_2SO_4). After evaporation of the solvents under vacuum, the crude product was purified by chromatography (ethyl acetate / methanol 98/2) yielding the desired product as a yellow oil (620 mg, 1.65 mmol, 82 %). ^{1}H-NMR (500,10 MHz, $CDCl_3$): δ 8.02 (d, ^{4}J = 1.4 Hz, 1H), 7.52 (d, ^{4}J = 1.4 Hz, 1H), 7.35 (d, ^{3}J = 9.5 Hz, 2H), 6.65 (d, ^{3}J = 9.5 Hz, 2H), 4.81 (d, ^{3}J = 5 Hz, 2H), 3.97 (s, 3H), 3.6 (m, 21H), 3.51 (m, 4H), 3.35 (s, 6H); ^{13}C-NMR (125.75 MHz, $CDCl_3$): δ 165.56, 160.37, 148.90, 147.20, 134.64, 133.74, 125.68, 125.07, 111.65, 108.05, 97.86, 72.12, 70.93, 70.86, 70.79, 68.53, 64.72, 59.25, 53.12, 51.03.

4. In a 50 mL round bottom flask under argon, **3** (300 mg, 0.52 mmol, 1 eq) was dissolved in THF (20 mL) and triethylamine (157 mg, 1.56 mmol, 3eq) and the mixture was cooled down to 0°C. A solution of methanesulfonyl chloride (72 mg, 0.63 mmol, 1.2 eq) in THF (5 mL) was added dropwise and the mixture was stirred at RT for 2 h. After epavoration of the solvent, the residue was dissolved in dichloromethane (50 mL), washed with water (3 x 100 mL), and dried (Na_2SO_4). After evaporation of the

solvents under vacuum, the crude product was purified by chromatography (ethyl acetate / methanol 98/2) to afford the desired product as a yellow oil (254 mg, 0.39 mmol, 75 %). ^{1}H-NMR (500,10 MHz, $CDCl_3$): 8.09 (d, ^{4}J = 1.4 Hz, 1H), 7.64 (d, ^{4}J = 1.4 Hz, 1H), 7.37 (d, ^{3}J = 9.1 Hz, 2H), 6.67 (d, ^{3}J = 9.1 Hz, 2H), 5.37 (s, 2H), 3.98 (s, 3H), 3.6 (m, 20H), 3.51 (m, 4H), 3.35 (s, 6H), 3.13 (s, 3H); ^{13}C-NMR (125.75 MHz, $CDCl_3$): δ 165.22, 154.52, 149.03, 147.90, 135.40, 133.85, 126.61, 126.21, 111.71, 99.02, 84.92, 72.11, 70.97, 70.93, 70.85, 70.79, 68.51, 59.24, 53.29, 51.06, 38.26. LRMS: m/z = 653 $[M+H]^+$, 675 $[M+Na]^+$

5. To a solution of **TACN,3HCl** (21 mg, 0.16 mmol, 1 eq) in dry MeCN (20 mL) was added the mesylate derivative **4** (430 mg, 0.66 mmol, 4 eq), sodium iodide (23 mg, 0.16 mmol, 1eq) and dry Na_2CO_3 (52 mg, 0.49 mmol, 3 eq). The resulting mixture was heated at reflux for 6 d and then filtered off. The filtrate was concentrated in vacuo and the oily residue was partitioned between water (50 mL) and CH_2Cl_2 (50 mL). The aqueous layer was extracted with CH_2Cl_2 (2 × 25 mL). The organic phases were combined, dried over Na_2SO_4 filtered and concentrated in vacuo. The crude material was purified by flash chromatography (DCM/Acetone/Methanol/Water 78/10/10/2 then 67/15/15/3) yielding a yellow oil (151 mg, 0.08 mmol, 51%). ^{1}H-NMR (500.10 MHz, $CDCl_3$): 7.97 (s, 3H), 7.33 (s, 3H), 7.24 (d, ^{3}J = 8.9 Hz, 6H), 6.64 (d, ^{3}J = 8.9 Hz, 6H), 4.29 (s, 6H), 3.88 (s, 9H), 3.60 (m, 60H), 3.51 (m, 12H), 3.34 (s, 18H), 3.28 (s, 12H). ^{13}C-NMR (125.75 MHz, $CDCl_3$): 165.1, 156.5, 148.8, 147.6, 134.7, 133.7, 128.0, 126.0, 111.4, 107.7, 98.5, 84.8, 71.9, 70.8, 70.7, 70.6, 68.4, 60.9, 59.1, 52.9, 50.9. HRMS *m/z*: $[C_{96}H_{136}N_9O_{24}]^+$ = 1798.9631 (calcd. 1798.9693).

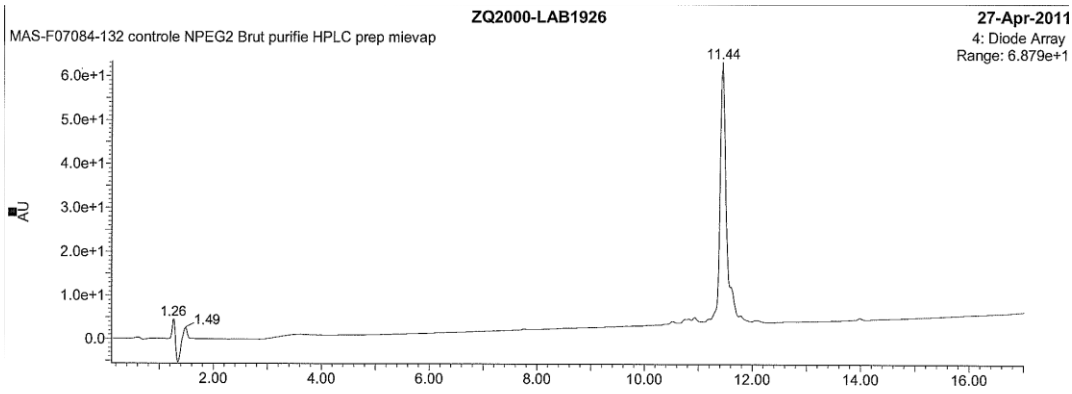

Figure S1. Semi-preparative HPLC chromatogram analysis of **5** (retention time, rt = 11.44 min).

L^2: To a solution of triester precursor **5** (110 mg, 0.060 mmol) in EtOH (15 mL) was added a NaOH 6M aqueous solution (15 mL) and the mixture was stirred at RT for 1 h. The organic solvent was evaporated, the aqueous phase was extended to 50 mL, and extracted with EtOAc (2 × 25 mL). After acidification to pH 1-2 (HCl (10%) solution), a second extraction was carried out with CH_2Cl_2 (3 × 25 mL). The organic phases were combined, dried over Na_2SO_4, filtered and concentrated in vacuo. The desired product is obtained as a yellow solid and was further engaged in the next step without further purification (100 mg 0.055mmol, 93%).

Yb^2: To a suspension of free ligand **L^2** (100 mg, 0.055 mmol, 1 eq) and K_2CO_3 (24 mg, 0.17 mmol, 3.1 eq) in dry MeCN (60 mL) was added $YbCl_3.6H_2O$ (21 mg,0.17 mmol, 3 eq). The solution was heated at 50°C for 12 h under inert atmosphere. The mixture was then cooled down to room temperature, filtered off and the filtrate was concentrated in vacuo. Purifications of the complexes were carried out by dialysis in water. After dialysis, the aqueous solution was extracted with dichloromethane (3 x 20 mL). The organic phases were combined, dried over Na_2SO_4, filtered and concentrated in vacuo yielding the desired complex as an orange solid (99 mg, 0.051 mmol, 91%). UV-vis (H_2O) λ_{max} = 364 nm (ε =34500 L.mol^{-1}.cm^{-1}), λ = 400 nm (ε =31000 L.mol^{-1}.cm^{-1}); HRMS *m/z*: $[C_{93}H_{127}N_9O_{24}Yb]^+$ = 1927.8341 (calcd. 1927.8381).

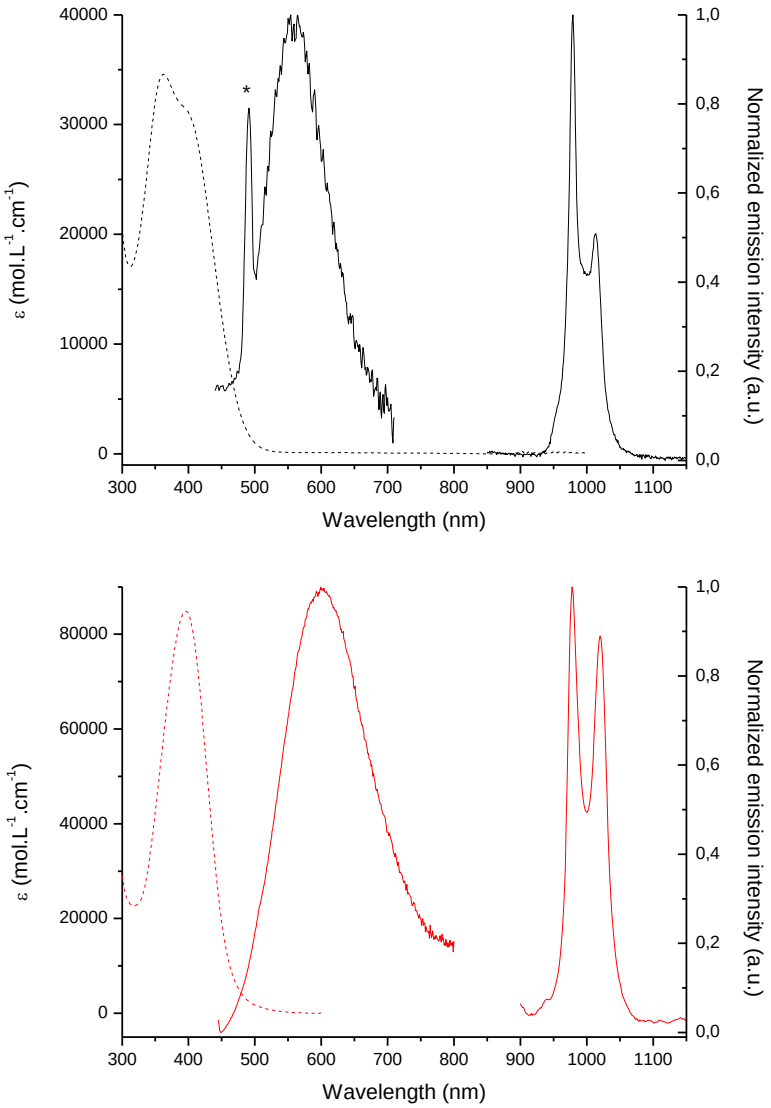

Figure S2. Absorption (…) and emission (-, λ^{ex} = 365 nm) spectra of **Yb^2** (black) and **Yb^1** (red) in diluted water solution. (*) Water scattering peak.

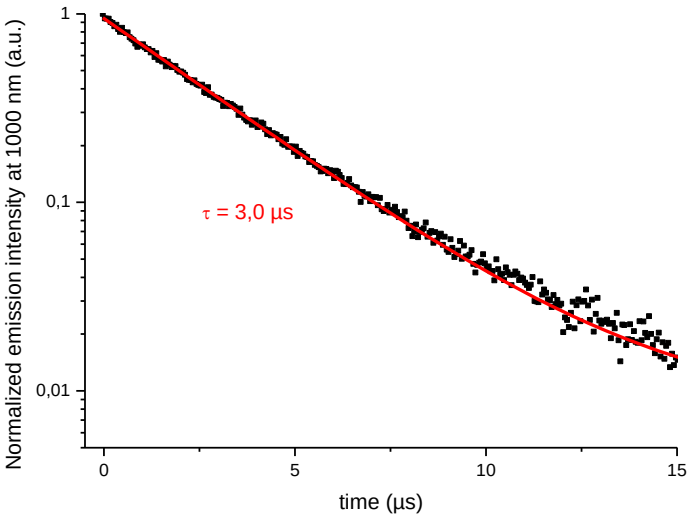

Figure S3. Experimental emission decay at 1000 nm for **Yb^2** in water solution (λ^{ex} =400 nm, ■). The best fit to a single exponential decay is shown in red, the decay is perfectly mono-exponential confirming that only one species is present under these conditions.

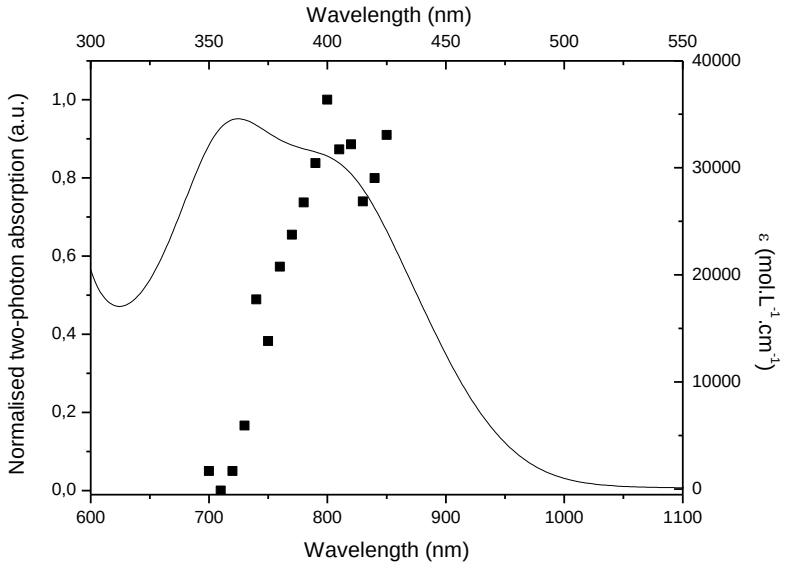

Figure S4. Two-photon excitation spectrum of **Yb^2** in water (■, lower abscissa). Superimposed on this plot is the single absorption spectrum (—, upper abscissa).

Luminescence. The luminescence spectra were measured using a Horiba-Jobin Yvon Fluorolog-3® spectrofluorimeter, equipped with a three slit double grating excitation and emission monochromator with dispersions of 2.1 nm/mm (1200 grooves/mm). The steady-state luminescence was excited by unpolarized light from a 450W xenon CW lamp and detected at an angle of 90° for diluted solution measurements (10

mm quartz cuvette) by a red-sensitive Hamamatsu R928 photomultiplier tube. Spectra were reference corrected for both the excitation source light intensity variation (lamp and grating) and the emission spectral response (detector and grating). Uncorrected near infra-red spectra were recorder using a liquid nitrogen cooled, solid Indium/Gallium/Arsenic detector (850-1600 nm). For luminescence lifetimes, the sample was excited using a pulsed Nd:YAG laser (SpectraPhysics), operating at 10 Hz. Light emitted at right angles to the excitation beam was focused onto the slits of a monochromator (PTI120), which was used to select the appropriate wavelength. The growth and decay of the luminescence at selected wavelengths was detected using a germanium photodiode (Edinburgh Instruments, EI-P) and recorded using a digital oscilloscope (Tektronix TDS320) before being transferred to a PC for analysis. Luminescence lifetimes were obtained by iterative reconvolution of the detector response (obtained by using a scatterer) with exponential components for growth and decay of the metal-centered luminescence, using a spreadsheet running in Microsoft Excel.

Two-photon excited luminescence measurements. The TPA cross-section spectrum was obtained by up-conversion luminescence using a Ti:sapphire femtosecond laser in the range 700-900 nm. The excitation beam (5 mm diameter) is focalized with a lens (focal length 10 cm) at the middle of the 10-mm cell. Emitted light was collected at 90° and was focused into an optical fiber (diameter 600 μm) connected to an Ocean Optics S2000 spectrometer. The incident beam intensity was adjusted to 50 mW in order to ensure an intensity-squared dependence of the luminescence over the whole spectral range. The detector integration time was fixed to 1s. Calibration of the spectra was performed by comparison with the published 700-900 nm Coumarin-307 two-photon absorption spectrum[3] (quantum yield = 0.56 in ethanol). The measurements were done at room temperature in dichloromethane and at a concentration of 10^{-4} M.

Microscopy imaging using commercial microscopes. Fixed and stained cells (as described below) were used without further rinsing for the imaging with the available commercial wide field epifluorescence and laser scanning multiphoton microscopes. The selective imaging of the ILCT emission band in epifluorescence mode was performed with the inverted wide field microscope (Zeiss, Axiovert 200M), equipped with the HBO 100 Hg lamp, Plan-Apochromat 63x/1.4 oil immersion objective and FITC epifluorescence filterset (HE38) BP450-490, FT495, BP 500-550, B/W CCD camera (CoolSnap HQ2).

The two-photon imaging was realized with the laser scanning microscope Zeiss LSM510 NLO META equipped with the pulsed femtosecond Ti:Sa laser (Tsunami, Spectra-Physics GmbH, Germany) tuned to 760 nm radiation. The detection was performed with spectral PMT (491-673) in descanned mode. The pinhole was open to 1000 μm and reflected IR light was suppressed with the BG39 filter. The irradiation intensity on the sample was ca. 3 mW at 14% transmission of the acousto–optical modulator. The fluorescence was collected with the 63x/1.4 PlanApochromat oil immersion objective. The 512x512 pixels fluorescence images were recorded simultaneously with the transmission light images with the

electronic zoom 3x and line averaged 8 times in order to optimize the signal-to-noise ratio. The pixel dwell time was adjusted to the emission lifetime of **Yb^{1}**. Neither signal saturation nor significant photobleaching was induced during image acquisition.

Biological samples. T24 cells (a bladder carcinoma cell line, ATCC HTB-4) were cultured in RPMI 1640 medium supplemented with 10% fetal bovine serum and antibiotics. For imaging experiments, T24 cells were seeded at low density on 2-well Lab-Tek Chambered Coverglass (Dominique Dutscher, Brumath, France) grown for 24h until the ca. 70% confluence before being fixed for 10min with Ethanol 100% at -20°C, washed twice with PBS and incubated with **Yb^{1}** ca. 2.10^{-5} M) for 40 min. Fixed cells conserve the appearance of living cells but possess more permeable cell membrane.

Mice brain preparation. 8-weeks old C57BL/6 mice obtained from our breeding facility were deeply anesthetized before being intracardiacally perfused with **Yb^{2}** dissolved in 0.1M phosphate buffer (PB, pH 7.4) (10 mL, c = 10^{-4} M). After perfusion, brains were quickly dissected and post-fixed for 4 hours in 4% paraformaldehyde (in 0.1M PB) and washed 3 times in Phosphate-buffered saline (pH 7.4). 100µm-thick brain slices were made using a a Vibratome (Integraslice 7550 PSDS, Campden Instruments), and stored in PBS until imaging was performed.

***NIR*-to-*NIR* Microscopy set up and validation.** Two-photon NIR-to-NIR microscopy imaging was performed using a femto-second tunable Ti:sapphire laser (100 fs, 80 MHz) excitation source, which the excitation wavelength fixed at 760 nm. This wavelength is the best compromise between the maximum of excitation for the molecule and the better signal to background obtained after rejection of the incident laser light.

The excitation was reflected on a dichroic beamsplitter (FF720-SDi01, Semrock) with short and long wave pass capability (transmission around 1000nm: 65%). The beam was then focused by a high numerical aperture objective (NA 1.15, x40) (Nikon), also used to collect the two-photon epi-fluorescence signal from the sample. The emission, detected by avalanche photodiodes, was first reflected on an interference filter tilted at 45° (800DF50, Omega Optical) and furthermore filtered spectrally around 1000 nm in order to avoid any scattering light from the incident laser (1000DF50, Omega Optical). The image of the sample was performed by galvanometric scanning, with a rate of typically one image every 1 to 2 seconds. The image was obtained by a descanning of the signal through the objective and galvanometric mirrors. The separation of the incident and detected beams was done before the galvanometric mirrors by the FF720-SDi01-dichroic beamsplitter.

The position of the focus position was controlled using a piezo-electric holder for the objective. A spectrum of emission could also be measured using a spectrometer at the exit of the microscope.

Penetration depth measurements on Intralipids Intralipids solutions of different concentration (10%, 15%, 20%) were prepared from a Intralipids-20% stock solution (Intralipid^{TM} Kabivitrum Inc.) diluted in

pure water. The **Yb**[1] complex was dissolved in the Intralipids solutions with a typical concentration of 10^{-4} M. A drop of the solution was directly deposited on a microscope coverslip. The initial focus (Z = 0 μm) was set at the interface between glass and solution. The focus was then controlled such as so enter progressively in the solution with 500 nm steps in the Z depth direction, recording the signal until a depth of Z = 300 μm.

NIR-to-NIR imaging in thick tissue slices from stained mouse brains. The tissue slice was directly positioned between glass slide and coverslip. Z-stacks images were obtained by performing an image every Z = 1 μm depth penetration step in the sample. Images of 100 μm x 100 μm were obtained with a sampling of 200 x 200 pixels, with an integration time of 50 μs per pixel, which leads to an imaging rate of about 1 image every 2 seconds. 3 accumulations per images were performed to ensure a correct signal to noise ratio. The incident power (760 nm incident wavelength) at the entrance of the microscope was set at 40 mW for the 610 nm detection wavelength and increased to 250 mW for 1000 nm detection. This leads to powers around respectively 4 mW and 25 mW at the focal spot of the objective. These powers were still low enough to not induce photodamage to the sample.

---

[1] A. D'Aléo, A. Picot, A. Beeby, J. A. G. Williams, B. Le Guennic, C. Andraud, O. Maury, *Inorg. Chem.* **2008**, *47*, 10258-10268; b) A. D'Aléo, A. Picot, P. L. Baldeck, C. Andraud, O. Maury, *Inorg. Chem.* **2008**, *47*, 10269-10279.

[2] A. Bourdolle, M. Allali, J.-C. Mulatier, B. Le Guennic, J. Zwier, P.L. Baldeck, J.C.G. Bünzli, C. Andraud, L. Lamarque, O. Maury, *Inorg. Chem.* **2011**, *50*, 4987-4999.

[3] C. Xu, W. W. Webb, *J. Opt. Soc. Am. B* **1996**, *13*, 481-491.